3-D wave-equation prestack imaging under salt

Biondo Biondi, Marie Prucha, Paul Sava, Stanford University*

SUMMARY

For the SEG-EAGE salt data set, common-azimuth migration produces better images in the subsalt than single-arrival Kirchhoff migration, at a similar computational cost. Subsalt reflectors are better imaged and the typical Kirchhoff artifacts caused by severe multipathing disappear. We show how angle-domain Common Image Gathers (CIG) can be easily extracted from prestack wavefield downward continued using wave-equation methods. These CIG gathers can be used to estimate the velocity function and analyze reflection amplitude as a function of aperture angle (AVA). A complete wave-equation imaging procedure that includes: migration, migration velocity analysis, and AVA analysis, can thus be applied to study reservoirs below complex overburden. This procedure should be more accurate and reliable than conventional Kirchhoff procedures when severe multipathing affects reflections.

INTRODUCTION

Kirchhoff migration methods often fail to produce satisfactory images of reflectors below complex overburden because they do not handle correctly multipathing of the reflected energy. When the wavefield is severely distorted by a salt body, or other complex velocity structure, the computation of the multivalued Green functions required by Kirchhoff methods is challenging. Further, even if we were able to compute the Green functions accurately and efficiently, the numerical integration of the wavefield over patchy and multivalued integration surfaces would be a difficult, and probably unreliable, task.

Wave-equation methods are an attractive and robust alternative to the complexities involved in extending Kirchhoff migration to handle correctly multipathing. However, full wave-equation 3-D prestack migration is still too computationally intensive to become a practical tool. Therefore, in the past few years we developed common-azimuth migration that is an approximation to full wave-equation 3-D prestack migration (Biondi and Palacharla, 1996; Biondi, 1997). It exploits the narrow-azimuth nature of marine data to reduce the computational cost by a large factor (20 to 50) with respect to full wave-equation 3-D prestack migration.

We applied common-azimuth migration to the narrow-azimuth subset of SEG-EAGE salt model (known as C3 Narrow-Azimuth classic data set or C3-NA) and compared the results with the results produced by a single-arrival Kirchhoff migration. The data were recorded on the realistic and complex salt-dome structure shown in Figure 1. In the subsalt areas, common-azimuth migration resolves the reflectors better than Kirchhoff migration, and yields an image with much fewer artifacts and spurious reflectors. The run times of common-azimuth migration and Kirchhoff migration were roughly the same. These results confirm the potentiality of wave-equation migration and give new impulse to our efforts to develop a complete wave-equation imaging (migration and velocity analysis) procedure for both structural and stratigraphic imaging.

To be a useful tool, a depth imaging procedure entails more than the production of a migrated cube. It also must enable the estimation of the velocity function and the prestack analysis of reflection amplitudes. Until recently, the lack of a simple and reliable method to extract prestack information from the results of wave-equation migration has been correctly perceived as a serious drawback. It curtailed the usefulness of wave-equation migration for both velocity estimation and Amplitude Versus Angle (AVA) analysis. In this paper we show a very simple method to overcome this problem. We slant stack the downward continued wavefield at each depth level and produce high-quality angle-domain Common Image Gathers (CIG) that display image amplitude as a function of the reflection angle. These gathers can be directly

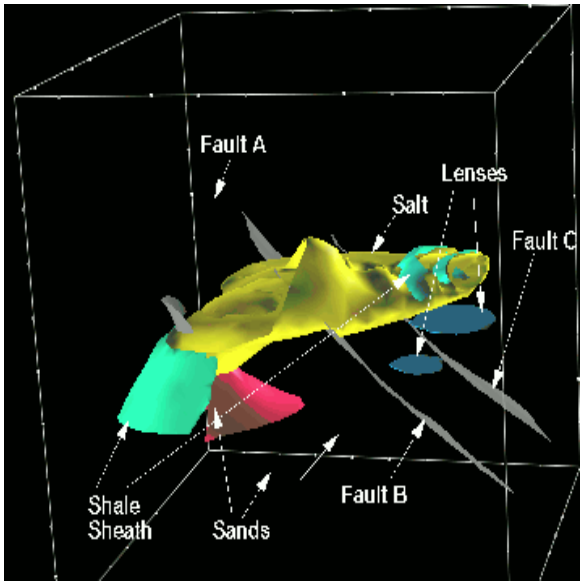

Figure 1: 3-D representation of the SEG-EAGE salt model.

used for AVA analysis, or for estimating migration velocity in a way similar to the common use of Kirchhoff-derived CIGs. The sensitivity to migration velocity errors of wave-equation CIGs is similar to the sensitivity of the CIGs obtained by migrating offset plane waves (Ottolini and Claerbout, 1984; Mosher et al., 1997). However, they are more accurate because they are based on a wavefield decomposition at depth and not at the surface.

Our ultimate goal is to build a complete and self-consistent wave-equation imaging procedure. An indispensable component of wave-equation imaging is a Wave-Equation Migration Velocity Analysis (WEMVA) method. In Biondi and Sava (1999) we present a WEMVA based on the linearization and inversion of downward continuation operators. WEMVA is more robust and stable than conventional ray-based MVAs because it can easily handle discontinuous velocity function and multipathing. The capability of performing both velocity analysis and AVA analysis by wave-equation methods is attractive because it opens the possibility, though still far from being reality, to perform AVA analysis in more complex areas than is possible today. For AVA analysis in complex areas, wave-equation methods have a crucial advantage over asymptotic methods; they can model correctly the amplitudes variations related to the focusing and defocusing of bandlimited wavefields caused by velocity variations.

SUBSALT MIGRATION: WAVE-EQUATION VS. KIRCHHOFF

The salt body in the model exhibits steep flanks near the crest and a rough surface on the top of the shelf. These characteristics cause severe distortions in the wavefield propagating through the salt. The reflectors below the salt area are thus poorly illuminated by data acquired with narrow-azimuth marine-like geometry. Consequently, the imaging of subsalt reflector is spotty even when using full-wave equation methods. Furthermore, deep dipping reflectors cannot be imaged because of the limited spatial extent of the data set. To reduce the computational cost of the modeling effort, the data were acquired on a dense grid only on a subset of the model. Good reference reflectors are: the bottom of the

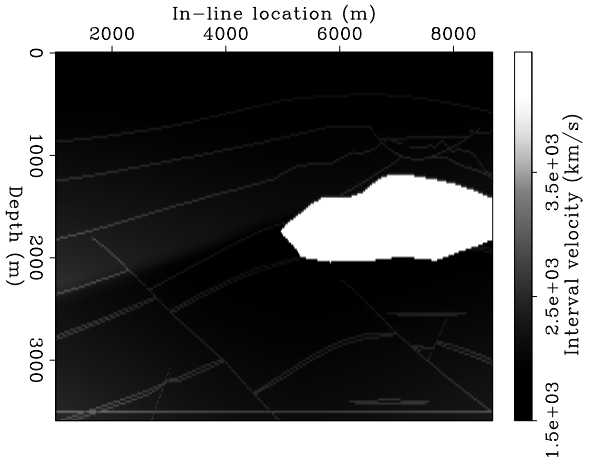

Figure 2: Velocity model at constant cross-line coordinate y=9,820 m.

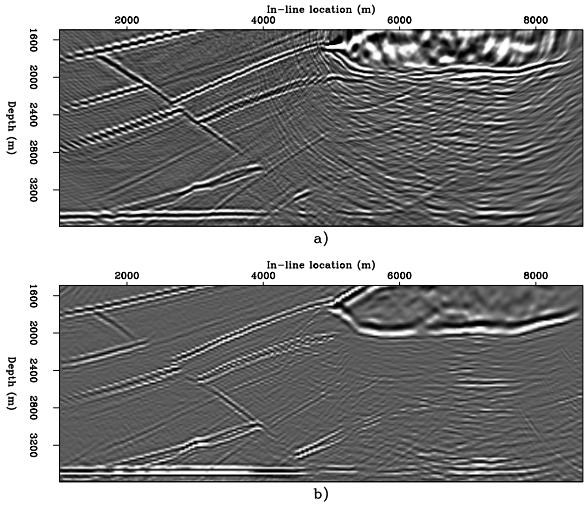

Figure 3: Kirchhoff migration (a) and common-azimuth migration (b) at constant cross-line coordinate y=9,820 m. Both sections are rendered using the same (98) percentile for clipping amplitudes.

salt, the flat strong reflector at the bottom of the model (not marked in Figure 1), and the two sand lenses marked as "Lenses" in Figure 1. The bottom of the salt can be imaged pretty well in most of the areas, with the exception of the root proximities, where the interfaces are steeply dipping.

Figure 2 shows the in-line section taken through the velocity cube at constant cross-line coordinate y=9,820 m . This section is interesting because it crosses both sand lenses in the subsalt. Further, between the lenses there is an anticlinal structure broken by converging normal faults that has some chances to be visible in the images because it is flattish. Figure 3 shows the subsalt images obtained by Kirchoff migration (top) and common-azimuth migration (bottom). The common-azimuth image is superior to the Kirchhoff image in several ways. First, the common-azimuth image lacks the strong coherent artifacts that makes the Kirchhoff image difficult to interpret. These artifacts are caused by partially coherent stacking of multipathing events along wrong trajectories. They are typical of Kirchhoff subsalt images, and can be only partially removed by a "smart" selection of the Kirchhoff summation surfaces, such as the ones suggested by the most-energetic arrival or shortest-path criteria (Nichols et al., 1998). Second, both lenses are interpretable from the common-azimuth image while in the Kirchhoff image they are either lost in the noise (top lens) or completely missing (bottom lens). Third, both the bottom of the salt and the basement are more continuous in the common-azimuth image.

Figure 4 shows the cross-line section taken through the velocity cube at constant in-line coordinate y=7,440 m. This cross-line section passes through the two subsalt lenses as the in-line section shown in Figure 2. Figure 5 shows the corresponding migrated images; Kirchhoff migration on the top and common-azimuth migration on the bottom. As before, the two lenses are clearly interpretable in the common-azimuth image, whereas they are not in the Kirchhoff image. However, in this case the central portion of the salt bottom is not perfectly imaged in either of the two images. This area is right below the deep canyons in the salt body visible in Figure 4. The steep flanks of the canyons, and the large velocity contrast between the salt body and the soft sediments filling the canyons, cause a severe distortion of the reflected wavefield. The bottom of the salt and the reflectors below, including the basement, are thus poorly illuminated. In the column below the canyons, the Kirchhoff image shows strong artifacts that could be easily interpreted as reflections. The common-azimuth image is much cleaner, although without interpretable coherent events.

The poor reflectors illumination below the canyons can be analyzed further by looking at the Common Image Gathers (CIG) displayed in

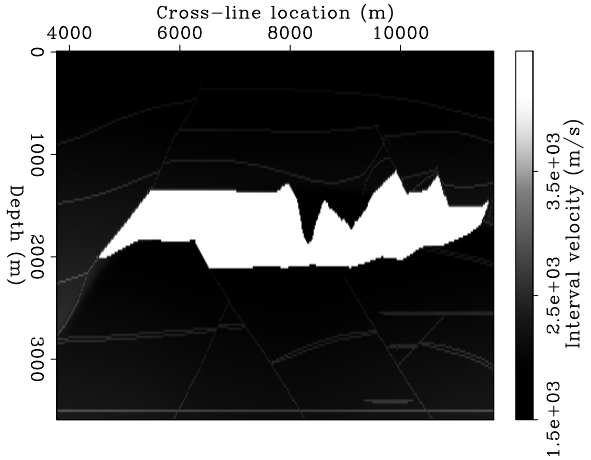

Figure 4: Velocity model at constant in-line coordinate x=7,440 m.

Figure 6. Next section describes how these gathers are extracted from the prestack downward continued wavefield. The gather on the left corresponds to a cross-line location right below the canyons; the one on the right is further toward the right. In both gathers, the images of the reflectors above the salt and the top-of-salt are well imaged and are aligned nicely along the offset ray parameter axis. In the gather on the right, the bottom of the salt, the shallower lens, the deeper lens, and the basement are also coherent and well aligned horizontally. But in the gather on the left, there is very little coherent energy below the salt.

ANGLE-DOMAIN CIG BY WAVE-EQUATION MIGRATION

When a complex velocity function induces multipathing and event triplication, angle-domain CIGs have advantages over offset-domain CIGs. Angle-domain CIGs can be easily extracted from downward-continued prestack data. Recorded 3-D seismic data can be organized as a function of midpoint coordinates (**m**) and offset coordinates (**h**). Prestack data are efficiently downward continued using the DSR equation in the frequency (ω) domain. Furthermore, since we either use 2-D downward continuation or 3-D common-azimuth downward continuation, the offset space is restricted to the in-line offset h_x , and thus we ex-

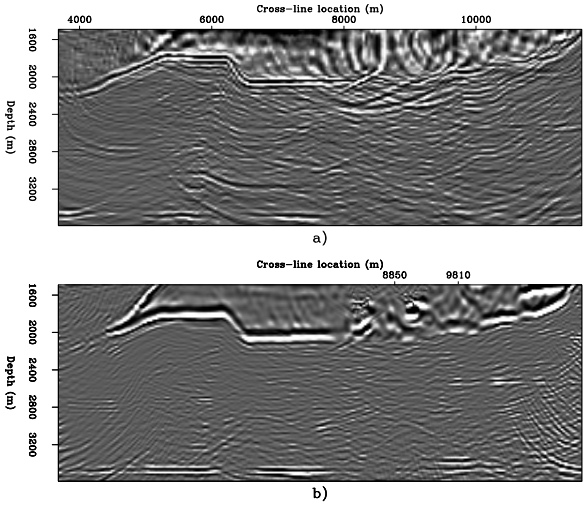

Figure 5: Kirchhoff migration (a) and common-azimuth migration (b) at constant in-line coordinate x=7,440 m. Both sections are rendered using the same (98) percentile for clipping amplitudes.

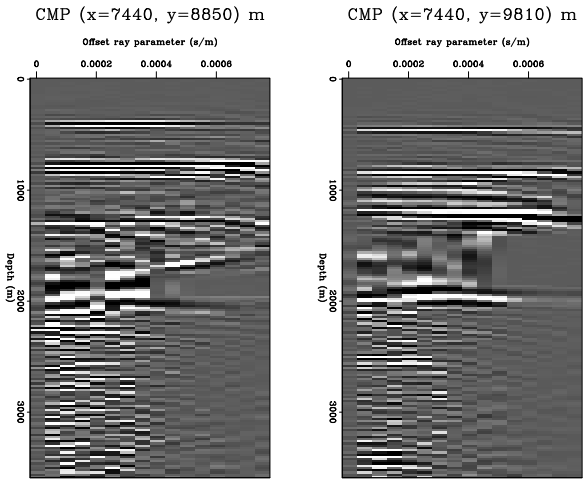

Figure 6: Angle-domain Common Image Gathers obtained by common-azimuth migration. The locations of these CIGs are marked on the in-line axis of the common-azimuth image shown in Figure 5

press the recorded wavefield as $P(\omega, \mathbf{m}, h_x; z = 0)$, where z is depth and z=0 indicates data recorded at the surface.

The prestack wavefield at depth is obtained by downward continuing the recorded data using the DSR, and is imaged by extracting the values at zero time

$$P(\omega, \mathbf{m}, h_x; z = 0) \overset{\text{DSR}}{\Longrightarrow} P(\omega, \mathbf{m}, h_x; z) \quad (1)$$

$$P(\omega, \mathbf{m}, h_x; z) \overset{Imaging}{\Longrightarrow} P(t = 0, \mathbf{m}, h_x; z) \quad (2)$$

The downward-continuation process focuses the wavefield towards zero offset (left panel in Figure 7) and if the continuation velocity is correct, a migrated image can be obtained by extracting the value of the wavefield at zero offset. However, the zero-offset wavefield has limited diagnostic information for velocity updating, and no information on the amplitude of the reflections versus reflection angle (AVA). We therefore perform a slant stack along the offset axis before imaging and obtain an image as a function of the offset ray parameter p_{hx}, as

$$P(\omega, \mathbf{m}, h_x; z = 0) \overset{\text{DSR}}{\Longrightarrow} P(\omega, \mathbf{m}, h_x; z) \quad (3)$$

$$P(\omega, \mathbf{m}, h_x; z) \overset{Slant\ stack}{\Longrightarrow} P(\tau, \mathbf{m}, p_{hx}; z) \quad (4)$$

$$P(\tau, \mathbf{m}, p_{hx}; z) \overset{Imaging}{\Longrightarrow} P(\tau = 0, \mathbf{m}, p_{hx}; z). \quad (5)$$

$$(6)$$

Angle-domain CIGs are subsets of $P(\tau = 0, \mathbf{m}, p_{hx}; z)$ at fixed midpoint location. The right panel in Figure 7 shows the angle-domain CIG gather corresponding to the downward-continued offset gather shown in the left panel. Notice that because in downward-continued offset gathers the energy is concentrated around zero offset, the slant stack decomposition does not suffer from the usual artifacts caused by the boundary conditions.

Strictly speaking, the CIG gathers obtained by the proposed procedure are function of the offset ray parameters p_{hx} and not of the aperture angle θ. However, p_{hx} is linked to θ by the following simple trigonometric relationship

$$\frac{\partial t}{\partial h} = p_{hx} = \frac{2 \sin\theta \cos\phi}{V(z, \mathbf{m})}, \quad (7)$$

where ϕ is the geological dip along the in-line direction and $V(z, \mathbf{m})$ is the velocity function.

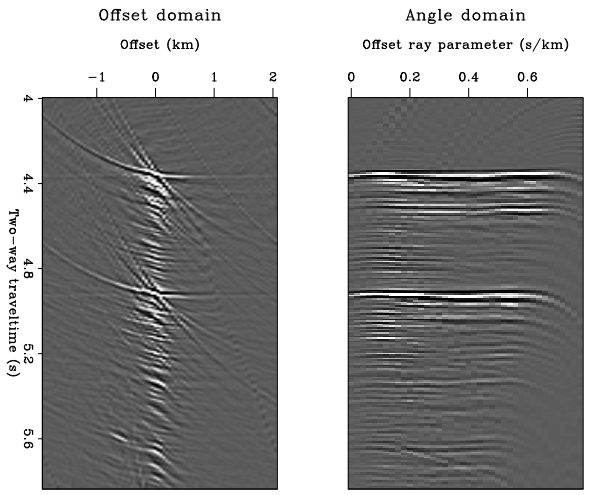

Figure 7: Left: Offset panel after downward continuation. Right: Angle-domain CIG

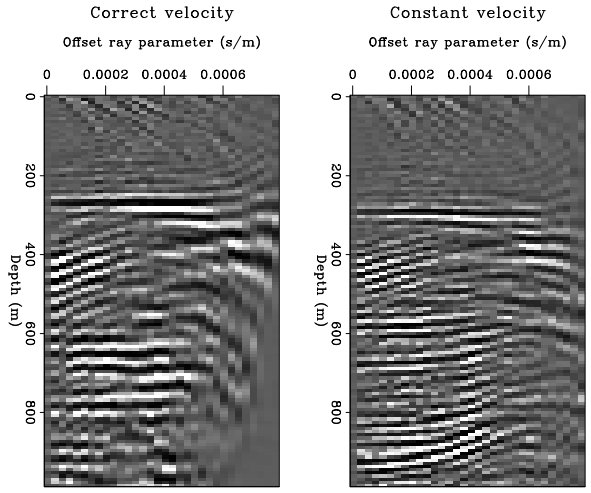

Figure 8: Left: Angle-domain CIG with correct velocity. Right: Angle-domain CIG with too low constant velocity.

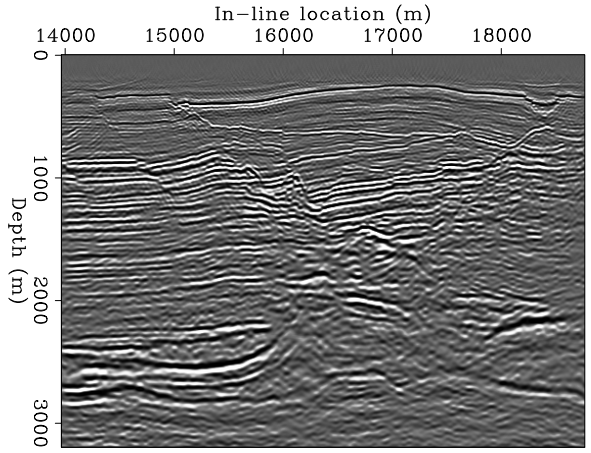

Figure 9: In-line section of 3-D migrated cube

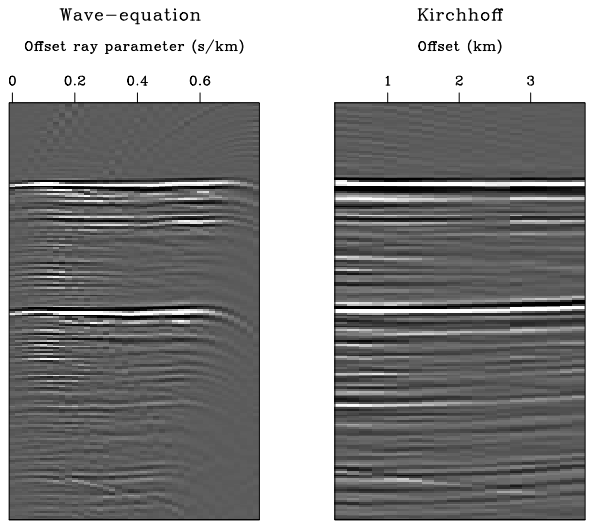

Figure 10: Left: Angle-domain CIG obtain by wave-equation migration. Right: Offset-domain CIG gather obtained by Kirchhoff migration

Angle-domain CIG and velocity

Angle-domain CIGs can be used to update the velocity function after migration similarly to the way that offset-domain CIGs are currently used or for wave-equation Migration Velocity Analysis (Biondi and Sava, 1999). As for offset-domain CIGs, if the velocity function is correct the reflections are aligned along the angle axis. If the velocity function is too low the reflections will smile upward; if the velocity function is too high the reflections will frown downward. This behavior is demonstrated by the analysis of the gathers in Figure 8. The gathers were extracted from a 3-D prestack wavefield focused using common-azimuth downward continuation. The left gather was obtained using the correct velocity. The right gather was obtained using a low constant velocity. Figure 9 shows the inline migrated section that passes through the gather shown in Figure 8. Notice that the CIG gathers show only the first kilometer of the image.

Angle-domain CIG and AVA

Angle-domain CIG can also be used to analyze the reflectivity as a function of the reflection angle to estimate rock and fluid properties in the subsurface. This potential use is illustrated by the gathers shown in Figure 10. The left panel shows an angle-domain CIG gather while the right panel shows the corresponding offset-domain CIG gather obtained by an amplitude preserving Kirchhoff migration. The amplitude behavior as a function of offset ray parameter (left panel) is in qualitative agreement with the the amplitude behavior as a function of offset (right panel).

CONCLUSIONS

Common-azimuth migration produced better results in the subsalt than a single-arrival Kirchhoff migration. The subsalt reflectors are much more interpretable in the common-azimuth images than in the Kirchhoff images, both because the images are devoid of the typical subsalt Kirchhoff artifacts and because the reflectors themselves are better imaged. Although superior to Kirchhoff images, the common-azimuth images in the subsalt are not perfect. Sub-optimal images are probably caused by a combination of poor reflectors' illumination and inaccuracies in the migration procedure. The shortcomings of common-azimuth migration can be addressed by improving the common-azimuth approximations and the numerical approximations that we used for the subsalt example. The angle-domain CIGs extracted from the downward continued wavefield can be used to perform migration velocity analysis and AVA analysis in conjunction with wave-equation migration. This capability should lead to a substantial improvement in the analysis of reservoirs that lying below complex overburden.

REFERENCES

Biondi, B., and Palacharla, G., 1996, 3-D prestack migration of common-azimuth data: Geophysics, **61**, 1822–1832.

Biondi, B., and Sava, P., 1999, Wave-equation migration velocity analysis: 69th Ann. Internat. Meeting, Soc. Expl. Geophys., submitted.

Biondi, B., 1997, Azimuth moveout + coomon-azimuth migration: Cost-effective prestack depth imaging of marine data: 67th Annual Internat. Mtg., Soc. Expl. Geophys., Expanded Abstracts, 1375–1378.

Mosher, C. C., Foster, D. J., and Hassanzadeh, S., 1997, Common angle imaging with offset plane waves: 67th Annual Internat. Mtg., Soc. Expl. Geophys., Expanded Abstracts, 1379–1382.

Nichols, D. E., Farmer, P., and Palacharla, G., 1998, Improving prestack imaging by using a new ray selection method: 68th Annual Internat. Mtg., Soc. Expl. Geophys., Expanded Abstracts, 1546–1549.

Ottolini, R., and Claerbout, J. F., 1984, The migration of common-midpoint slant stacks: Geophysics, **49**, no. 03, 237–249.